

QUT Digital Repository:
<http://eprints.qut.edu.au/>



Frost, Ray L. and Keeffe, Eloise C. and Reddy, B. Jagannadha (2009) *An application of near-infrared and mid-infrared spectroscopy to the study of selected tellurite minerals: xocomecatlite, tlapallite and rodalquilarite.* *Transition Metal Chemistry*, 34(1). pp. 23-32.

© Copyright 2009 Springer

1
2
3
4
5
6
7
8
9
10
11
12
13
14
15
16
17
18
19
20
21
22
23
24
25
26
27
28
29
30
31
32
33
34

An application of near-infrared and mid-infrared spectroscopy to the study of selected tellurite minerals: xocomecatlite, tlapallite and rodalquilarite

Ray L. Frost, • B. Jagannadha Reddy, Eloise C. Keeffe

Inorganic Materials Research Program, School of Physical and Chemical Sciences, Queensland University of Technology, GPO Box 2434, Brisbane Queensland 4001, Australia.

Abstract

Near-infrared and mid-infrared spectra of three tellurite minerals have been investigated. The structure and spectral properties of two copper bearing xocomecatlite and tlapallite are compared with an iron bearing rodalquilarite mineral. Two prominent bands observed at 9855 and 9015 cm^{-1} are assigned to ${}^2\text{B}_{1g} \rightarrow {}^2\text{B}_{2g}$ and ${}^2\text{B}_{1g} \rightarrow {}^2\text{A}_{1g}$ transitions of Cu^{2+} ion in xocomecatlite. The cause of spectral distortion is the result of many cations of Ca, Pb, Cu and Zn in tlapallite mineral structure. Rodalquilarite is characterised by ferric ion absorption in the range 12300-8800 cm^{-1} .

Three water vibrational overtones are observed in xocomecatlite at 7140, 7075 and 6935 cm^{-1} where as in tlapallite bands are shifted to low wavenumbers at 7135, 7080 and 6830 cm^{-1} . The complexity of rodalquilarite spectrum increases with more number of overlapping bands in the near-infrared. The observation of intense absorption feature near 7200 cm^{-1} confirms strongly hydrogen bonding water molecules in xocomecatlite. Weak bands observed near 6375 and 6130 cm^{-1} in tellurites are attributed to the hydrogen bonding between $(\text{TeO}_3)^{2-}$ and H_2O . A number of overlapping bands in the low wave numbers 4800-4000 cm^{-1} are caused by combinational modes of tellurite ion. $(\text{TeO}_3)^{2-}$ stretching vibrations are characterized by three main absorptions at $\sim 1070, 780$ and 665 cm^{-1} .

• Author to whom correspondence should be addressed (r.frost@qut.edu.au)

35

36

37 **Keywords:** tellurites, xocomecatlite, tlapallite, rodalquilarite, Near-IR and Mid-
38 infrared spectroscopy, hydrogen bonds, $(\text{TeO}_3)^{2-}$, Cu^{2+} , Fe^{3+}

39

40 **Introduction**

41

42 Recent research efforts in our group have focussed on spectroscopic
43 characterisation (NIR, IR and Raman) of selenites and tellurites based on the limited
44 information available in literature. According to the formula and structure, selenites
45 and tellurites may be distributed into five groups: [1] (a) $\text{A}(\text{XO}_3)$, (b) $\text{A}(\text{XO}_3) \cdot x\text{H}_2\text{O}$,
46 (c) $\text{A}_2(\text{XO}_3)_3 \cdot x\text{H}_2\text{O}$, (d) $\text{A}_2(\text{X}_2\text{O}_5)$ and (e) $\text{A}(\text{X}_3\text{O}_8)$. Of the selenites, molybdomenite
47 is an example of type (a) chalcomenite, clinochalcomenite, cobaltomenite and
48 ahlfeldite are examples of type (b) and mandarinoite is an example of type (c). There
49 are no known examples of selenite minerals with formula (d) and (e). The tellurite
50 group, however, consists of minerals that can be categorised into each of the five
51 formula types. Tlapallite, xocomecatlite and rodalquilarite examples of type (a) and
52 other related minerals are fairbankite, balyakinite, plumbotellurite, mocktezumite,
53 magnolite and smirnite are examples of type (a); graemite, teineite and chalcoalite are
54 examples of type (b); zemmanite and emmonsite are examples of type (c); rajite and
55 denningite are examples of type (d) and spiroffite, winstanleyite, carlfreisite and
56 pingguite are examples of type (e). An additional group with alternate formula and
57 structure, is one in which the minerals contain water and/or OH units. The minerals:
58 rodalquilarite, sonoraite, cesbronite, guilleminite, marthozite, demesmaekerite and
59 haynesite are represented by this group. The two related minerals teineite
60 $\text{Cu}(\text{TeO}_3) \cdot 2\text{H}_2\text{O}$ [2-7] and graemite $\text{Cu}(\text{TeO}_3) \cdot \text{H}_2\text{O}$ [8, 9] are examples of hydrated
61 tellurites.

62

63 Other tellurite minerals like emmonsite, mackayite and sonoraite are often
64 found together in tellurite mineral deposits [10]. Teineite, graemite and some related
65 compounds have been synthesised [2, 11-13]. Related minerals kinichilite
66 $\text{Mg}_{0.5}[\text{Mn}^{2+}\text{Fe}^{3+}(\text{TeO}_3)_3]_4 \cdot 5\text{H}_2\text{O}$ [14] and emmonsite, $\text{Fe}_2^{3+}\text{Te}_3^{4+}\text{O}_9 \cdot 2\text{H}_2\text{O}$ are found in
67 the tellurium rich deposits of Mexico [15]. The importance of these tellurium bearing
68 minerals is their open framework structures with negatively charged surfaces and

69 zeolitic pores. Other tellurite minerals are cliffordite $\text{UTe}_3^{4+}\text{O}_9$ [16, 17] and
70 keystoneite $\text{Mg}_{0.5}[\text{Ni}^{2+}\text{Fe}^{3+}(\text{TeO}_3)_3]_4 \cdot 5\text{H}_2\text{O}$ [18, 19]. Tellurites are especially
71 appealing because they adopt a number of unusual coordination environments. The
72 usual form is TeO_3 pyramids like sulphites and selenites. They also form four-
73 coordinated $(\text{TeO}_4)^{4-}$ fragments with C_{2v} symmetry. Alternatively tellurites also adopt
74 a unique $(\text{TeO}_{3+1})^{4-}$ geometry [20-22], in which one of the axial sites of the
75 pseudotrigonal bipyramid is much longer than the other. Thus their coordination
76 chemistry is of interest since they should be a source of new and interesting solid state
77 phases. Two compounds, $\text{Ba}_2\text{Cu}_4\text{Te}_4\text{O}_{11}\text{Cl}_4$ and $\text{BaCu}_2\text{Te}_2\text{O}_6\text{Cl}_2$ containing tellurite
78 building blocks coordinated to copper and barium atoms have been isolated from
79 hydrothermal solvents [23]. The compounds contain two types of layers, one based on
80 copper oxides linked by Te_4O_{11} groups, and the other based on Cu_2Cl_4 units. The
81 tellurium atoms adopt the common TeO_{3+1} units or TeO_3 pyramids, and the oxygen-
82 coordinated copper atoms adopt a square planar CuO_4 arrangement.
83 The rich chemistry of tellurites has drawn our attention to investigate the spectroscopy
84 of copper bearing tellurites, naturally occurring minerals. We have selected two
85 copper bearing minerals xocomecatlite $\text{Cu}_3[(\text{OH})_4\text{TeO}_4]$, tlalallite
86 $\text{H}_6(\text{Ca,Pb})_2(\text{Cu,Zn})_3\text{SO}_4(\text{TeO}_3)_4\text{TeO}_6$ and one iron bearing tellurite mineral
87 rodalquilarite $\text{H}_3\text{Fe}_2(\text{TeO}_3)_4\text{Cl}$. An emission spectrogram of Mexican tlalallite
88 showed major amounts of copper, tellurium, calcium, and lead [24]. Xocomecatlite is
89 classified as orthorhombic system and Cu and Te are the major empirical contents
90 [25]. Rodalquilarite also belongs to the same group with Cu and Te as major
91 composition.

92
93 Raman spectroscopy has proven very useful for the study of minerals [26-36].
94 Near-infrared and mid-infrared spectroscopy has proven most useful for the study of
95 diagenetically related minerals, as many minerals often occur with many carbonate
96 minerals [27, 37-50]. In this paper, we present near-infrared and mid-infrared
97 measurements of three selected tellurite minerals and report the structure and spectral
98 properties. The spectra of two copper tellurites, xocomecatlite $\text{Cu}_3[(\text{OH})_4\text{TeO}_4]$ and
99 tlalallite $\text{H}_6(\text{Ca,Pb})_2(\text{Cu,Zn})_3\text{SO}_4(\text{TeO}_3)_4\text{TeO}_6$ are compared with that of iron bearing
100 rodalquilarite $\text{H}_3\text{Fe}_2(\text{TeO}_3)_4\text{Cl}$.

101

102 **Experimental**

103 Minerals

104 The minerals used in this work, their formula and origin are listed in Table 1.
105 The tellurite minerals obtained from Mineralogical Research Company, USA; (a)
106 xocomecatlite $\text{Cu}_3[(\text{OH})_4\text{TeO}_4]$ and tlapallite $\text{H}_6(\text{Ca,Pb})_2(\text{Cu,Zn})_3\text{SO}_4(\text{TeO}_3)_4\text{TeO}_6$
107 originated from Bambollita Mine, Moctezuma District, Sonora, Mexico where as
108 rodalquilarite $\text{H}_3\text{Fe}_2(\text{TeO}_3)_4\text{Cl}$ originated from Wendy Pit, El Indio Gold Mine,
109 Coquimbo, Chile. Anthony et al. reported the typical composition of these minerals
110 [10] 38.70% TeO_3 , 51.30% CuO , 2.40% ZnO and 8.00% H_2O xocomecatlite,
111 tlapallite: 5.20% SO_3 , 11.40% TeO_3 , 41.40% TeO_2 , 15.60% CuO , 0.80% ZnO and
112 8.30% CaO to be 5.20% SO_3 , 11.40% TeO_3 , 41.40% TeO_2 , 15.60% CuO , 0.80% ZnO
113 and 8.30% CaO and rodalquilarite: 72.85% TeO_2 , 18.45% Fe_2O_3 , 4.80% Cl , 4.50%
114 H_2O , 0.35% insol. and 1.08% $-\text{O} = \text{Cl}_2$.
115

116 Infrared and Near-infrared (NIR) spectroscopy

117 Infrared spectra were obtained using a Nicolet Nexus 870 FTIR spectrometer
118 with a smart endurance single bounce diamond ATR cell. Spectra over the 4000 to
119 525 cm^{-1} range were obtained by the co-addition of 64 scans with a resolution of 4
120 cm^{-1} and a mirror velocity of 0.6329 cm/s . NIR spectra were collected on a Nicolet
121 Nexus FT-IR spectrometer with a Nicolet Near-IR Fibreport accessory (Madison,
122 Wisconsin). A white light source was used, with a quartz beam splitter and TEC NIR
123 InGaAs detector. Spectra were obtained from 13 000 to 4000 cm^{-1} ($0.77\text{-}2.50\text{ }\mu\text{m}$) by
124 the co-addition of 64 scans at a spectral resolution of 8 cm^{-1} . A mirror velocity of
125 1.266 m sec^{-1} was used. The spectra were transformed using the Kubelka-Munk
126 algorithm to provide spectra for comparison with published absorption spectra.
127 Spectral manipulations, such as baseline correction, smoothing and normalisation,
128 were performed using the software package GRAMS (Galactic Industries
129 Corporation, NH, USA).

130 Band component analysis was undertaken using the Jandel 'Peakfit' (Erkrath,
131 Germany) software package which enabled the type of fitting function to be selected
132 and allows specific parameters to be fixed or varied accordingly. Band fitting was
133 done using a Lorentz-Gauss cross-product function with the minimum number of
134 component bands used for the fitting process. The Lorentz-Gauss ratio was

135 maintained at values greater than 0.7 and fitting was undertaken until reproducible
136 results were obtained with squared correlations (r^2) greater than 0.995. Band fitting
137 of the spectra is quite reliable providing there is some band separation or changes in
138 the spectral profile.

139

140 **Results and discussion**

141

142 **Near-infrared (NIR) spectroscopy**

143 The reflectance spectra of tellurites in the range 13000-4000 cm^{-1} show
144 diagnostic absorption bands related to d-d transitions and vibrational process
145 involving hydroxyl units. Bands in the electronic spectrum are broad and occur in
146 high wavenumbers where as the bands in the vibrational spectrum usually appear in
147 the low wavenumber region 7500-4000 cm^{-1} [51, 52]. Many of these absorption bands
148 are relatively broad and overlap. By the application of band component analysis the
149 spectral differences between the minerals are illustrated in plots showing major
150 absorption band positions. NIR spectral features are subdivided into three regions
151 (Figures 1 to 3): the first region is the high wavenumber region 12500-7500 cm^{-1} ;
152 spectra of the tellurites are shown in the Fig. 1. This is the region where characteristic
153 electronic bands are caused by d-d transitions. In the second region 7500-6500 cm^{-1}
154 bands are attributed to the first overtones of the fundamental OH stretching modes of
155 water. Bands in the third region 6500-4000 cm^{-1} appear due to the combinational
156 modes of OH stretching and bending modes and bands at $<4800 \text{ cm}^{-1}$ may be
157 attributed to the combinations of the stretching and deformation modes of tellurite/
158 tellurite ion.

159

160 *Electronic spectra: 12000-7500 cm^{-1} spectral region*

161

162 Transition metals are likely candidates for the source of bands observed in the
163 near-infrared region for these materials. For the study of spectral properties, three
164 minerals xocomecatlite, tlapallite and rodalquilarite selected from tellurite group
165 contain two different metal ions of copper and iron. Crystal field effects due to the
166 presence of transition metal cations (3d-ions) are significant in their spectra as
167 depicted in Figure 1. The dependence of composition on spectral properties is a key to

168 mineral identification and forms the basis for subdivision of the minerals in tellurite
169 group. The two minerals xocomecatlite $\text{Cu}_3[(\text{OH})_4\text{TeO}_4]$ and tlapallite
170 $\text{H}_6(\text{Ca,Pb})_2(\text{Cu,Zn})_3\text{SO}_4(\text{TeO}_3)_4\text{TeO}_6$ are characterised by Cu^{2+} bands in the electronic
171 spectrum of 12000-7500 cm^{-1} region (Figure 1). Cu^{2+} corresponds to the d^9
172 configuration and is considered with one unpaired electron. Hence there is one free
173 ion term 2D . The 2D term splits into ground state 2E_g and excited 2T_g state in
174 octahedral crystal field. But 2E_g is unstable and splits under the influence of Jahn-
175 Teller effect and 2T_g excited state also splits. Thus Cu^{2+} complexes never correspond
176 to the regular octahedron; instead six-fold coordination (4+2) always occurs in the
177 form of an elongated octahedron. As a result of distortion of octahedral symmetry
178 copper complexes usually show three bands relating to $^2B_{1g} \rightarrow ^2A_{1g}$, $^2B_{1g} \rightarrow ^2B_{2g}$ and
179 $^2B_{1g} \rightarrow ^2E_g$ transitions [53, 54]. The first two transitions are very close in energy and
180 often appear in the form of one broad band profile in the near-infrared and third band
181 may be observed in the visible region [55]. For connellite $\text{Cu}_{19}(\text{SO}_4)\text{Cl}_4(\text{OH})_{32}\cdot 3\text{H}_2\text{O}$
182 two transitions $^2B_{1g} \rightarrow ^2A_{1g}$ and $^2B_{1g} \rightarrow ^2B_{2g}$ have been reported at 8335 and 12050
183 cm^{-1} [56]. NIR bands have been observed in copper bearing silicate, shattuckite
184 $\text{Cu}_8(\text{Si}_4\text{O}_{11})\text{OH}_4$ at 8330 and 10695 cm^{-1} [57]. Near infrared spectroscopic study of
185 smithsonite minerals shows bands at 8050 and 10310 cm^{-1} were attributed to Cu(II)
186 ion for smithsonite, a Cu bearing-carbonate mineral from Namibia [58]. A single
187 intense band reported for Cu (II) in conichalcite [$\text{CaCuAsO}_4\text{OH}$] at 8585 cm^{-1} was
188 assigned to $^2B_{1g} \rightarrow ^2A_{1g}$ transition [41].

189 In the present study the involvement of cations, like Ca, Pb, Zn and mainly the
190 two transition metal ions of Cu and Fe show the effect of variable band positions and
191 intensities. On account of these factors the application of band component analysis
192 permits minerals to be distinguished. Most of the bands are broad in nature and some
193 of them are unsymmetrical with shoulders too. The resolution of each band by peak fit
194 analysis give rises to a number of components of which main components are
195 recognized, analyzed and interpreted. The electronic spectrum of xocomecatlite shows
196 a broad profile in which a number of component bands indicates distortion of
197 symmetry for Cu^{2+} [53,54]. Four component bands are resolved at 865, 922, 1014 and
198 1109 nm (11560, 10835, 9855 and 9015 cm^{-1}). The shoulder appeared on low
199 wavenumber side at 1109 nm (9015 cm^{-1}) is identified as $^2B_{1g} \rightarrow ^2A_{1g}$ transition. The
200 sharp band at 1014 nm (9855 cm^{-1}) displayed with two components at 865 and 922

201 nm (11560 and 10835 cm^{-1}) is assigned to ${}^2\text{B}_{1g} \rightarrow {}^2\text{B}_{2g}$ transition. Generally two
 202 closely lying Cu^{2+} bands appear in NIR [57,58]. The effect of other cations of Ca, Pb
 203 and Zn in tlapallite is the cause for different band positions with greater separation
 204 (Figure 1). The band centred at 935 nm (10690 cm^{-1}) with two components on either
 205 side at 870 and 1016 nm (11490 and 9840 cm^{-1}) is assigned to ${}^2\text{B}_{1g} \rightarrow {}^2\text{B}_{2g}$ transition.
 206 Interestingly it can be noticed that the second band is dissipated to low wavenumbers
 207 at 8200-7400 cm^{-1} in the form of weak envelope (Figure 2b). This broad feature
 208 shows a weak band at 1313 nm (7615 cm^{-1}) with a component at 7990 cm^{-1}
 209 attributable to ${}^2\text{B}_{1g} \rightarrow {}^2\text{A}_{1g}$ transition. The result of spectral variations is the effect of
 210 many other cations in the mineral structure which is also evident from chemical
 211 analysis of tlapallite [10]. The nature of the electronic spectrum of rodalquilarite
 212 $\text{H}_3\text{Fe}_2(\text{TeO}_3)_4\text{Cl}$ is different from Cu-bearing tlapallite and xocomecatlite minerals
 213 since ferric iron is involved in rodalquilarite mineral structure. Crystal field bands of
 214 Fe^{3+} minerals show two broad bands at lower energies (labelled as ${}^4\text{T}_{1g}$ and ${}^4\text{T}_{2g}$) and
 215 a pair of bands in the UV region. Rossman report on the correlation of optical
 216 absorption intensities and magnetic moments of Fe^{3+} minerals demonstrates the
 217 dependence of optical absorption intensity and antiferromagnetic interactions in the
 218 host phase [59]. ${}^6\text{A}_{1g} \rightarrow {}^4\text{T}_{1g}$ transition band in minerals that contain ferric ion sites
 219 has been reported; 853 nm (11710 cm^{-1}) in andradite $\text{Ca}_3\text{Fe}_2(\text{SiO}_4)_3$ [61], hematite
 220 Fe_2O_3 855 nm (11695 cm^{-1}), and 917 nm (10895 cm^{-1}) in lepidocrocite $\text{FeO}(\text{OH})$
 221 [61,62]. Ferric ion is responsible for the origin of the observed transition in Figure 1c
 222 (12300-8800 cm^{-1}). Fe^{3+} ion transitions are from ground ${}^6\text{A}_{1g}$ state to different quartet
 223 states known as spin forbidden transitions. The observed feature is defined by two
 224 components in rodalquilarite spectrum at 890 and 956 nm (11230 and 10460 cm^{-1}) is
 225 assigned to ${}^6\text{A}_{1g} \rightarrow {}^4\text{T}_{1g}$ transition of Fe^{3+} ion. Both, tlapallite and rodalquilarite
 226 exhibit similar features in the range 8300-7400 cm^{-1} . A group of weak bands in
 227 rodalquilarite spectrum centred at 7615 cm^{-1} might be the cause of minor amounts of
 228 copper ion in the mineral structure.

229

230

231 *NIR spectra: 7000-6500 cm^{-1} spectral region*

232 Water and or OH^- commonly occur in minerals. The mineral spectra in the
 233 near-infrared and mid-infrared (7200-2000 cm^{-1}) may be used to estimate the absolute

234 or relative amount of water in minerals [60]. Band component analyses of the spectra
235 of three tellurite minerals in the 7500-6500 cm^{-1} region are shown in Figure 2.
236 Xocomecatlite and tlapallite from Mexico exhibit nearly similar spectra in which OH
237 overtone bands result from the structural water in the minerals. The overtone bands of
238 water have been observed in reflectance spectra of many H_2O -bearing minerals. The
239 first overtones of OH stretches occur at 7150 cm^{-1} and the combinations of the H-O-H
240 bend with OH stretches are found near 5250 cm^{-1} [61]. In xocomecatlite three bands
241 are observed at 7140, 7075 and 6935 cm^{-1} and one group of weak bands are observed
242 at 6825, 6755 and 6685 cm^{-1} . The band at 6935 cm^{-1} is significantly broader. This
243 width is due to the combination of a number of bands contributing to the band
244 envelope. The bands at 7075 and 7140 cm^{-1} are sharp because these bands are the first
245 overtone of the fundamental. The band at 7100 cm^{-1} is also attributed to an overtone
246 of fundamental vibrations. It must be remembered that in NIR spectroscopy all
247 overtones and combinations are allowed. So it is not unusual to observe three sharp
248 overtones. For tlapallite these bands are shifted to low wavenumbers at 7135, 7080,
249 6830 and 6640 cm^{-1} . In both the minerals the bands in the 7240- 6900 cm^{-1} region are
250 attributed to the first overtones of ν_{OH} vibrations observed in the range 3650-2200
251 cm^{-1} for water in minerals (Figures 4a to 4c). The complexity of rodalquilarite
252 spectrum increases with more number of overlapping bands at 7185, 7010, 6855 and
253 6765 cm^{-1} and two weak bands at 6660 and 6545 cm^{-1} . The complexity of the
254 spectrum is attributed to the presence of protons in the mineral structure. Thus
255 formation of H_3O^+ units and OH units can be formed. Further complexity is attributed
256 to the non-equivalence of the $(\text{TeO}_3)^{2-}$ units in the rodalquilarite structure. These
257 absorptions are recognised as the overtones of water ($2 \nu_3$ and $2 \nu_1$). Weak bands
258 observed near 6375 and 6130 cm^{-1} in tellurites may be attributed to the hydrogen
259 bonding between $(\text{TeO}_3)^{2-}$ and H_2O . The observation of intense absorption feature
260 centred around 7200 cm^{-1} confirms molecular water in tellurite minerals/shows
261 strongly hydrogen bonding water molecules in the minerals and is more significant in
262 xocomecatlite.

263

264

265 *NIR spectra: 6500-4000 cm^{-1} spectral region*

266

267 There are three sharp absorption groups in 5400-4000 cm^{-1} region (Figure 3).
268 Three prominent peaks are observed in xocomecatlite at 5150, 4555 and 4115 cm^{-1} .
269 These positions vary a little in tlallallite but bands are overlapped with more number
270 of components at 5165, 4550 and 4025 cm^{-1} . The spectrum of rodalquilarite is altered
271 mainly due to the presence of iron in the mineral and the absorption profile is more
272 complex with many overlapping bands at 5200, 4610, 4305, 4110 and 4050 cm^{-1} . The
273 appearance of the most intense peak near 5150 cm^{-1} with a pair of weak shoulders on
274 the high wavenumbers at $\sim 5650 \text{ cm}^{-1}$ is a common feature in all the spectra and is
275 related to the combinations of OH vibrations of water molecules, (ν_3/ν_1) [ν_3 or ν_1] and
276 bending vibrations ν_2 ($\delta \text{ H}_2\text{O}$). This feature further supports the presence of molecular
277 water in tellurites. Investigations on near-infrared spectra of selenites shows bands in
278 the region 7500-4000 are assigned to the overtones of water stretching vibrations and
279 the vibrational units of $(\text{SeO}_3)^{2-}$ and this study of selenite minerals; chalcomenite,
280 clinochalcomenite and cobaltomenite by Frost et al. [62], reveals the assignment of
281 the sharp band observed at 5170 cm^{-1} along with a low intensity band near 5600 cm^{-1}
282 are derived from the combinational modes of OH vibrations of H_2O molecules.

283

284 A number of overlapping bands in the low wave numbers 4800-4000 cm^{-1} are
285 caused by combinational modes of $(\text{TeO}_3)^{2-}$. Distinct patterns displayed by these
286 minerals as shown in Figure 3 are utilised for rapid identification of the specific type
287 of tellurite minerals. The assignment of the bands of three tellurite minerals reported
288 in Table 2 and is comparable with selenites as both are related to one group.

289

290 **Infrared spectroscopy**

291

292 Many of the naturally occurring minerals, both hydrous and anhydrous,
293 contain, molecular water, hydroxyl anions or even excess protons. In particular, water
294 stored in their structures as OH or H_2O can dramatically affect geologic processes.
295 Water also plays a crucial role within the Earth's crust and at greater depth's beneath
296 the crust [63]. Intensity and shape of absorption bands in minerals depend on the
297 composition and structure, albedo and particle size [64]. The influence of hydrogen
298 bonding strongly depends on OH stretching bands [65]. Molecular water (C_{2v}) is
299 characterised by three fundamentals: $\nu_{1\text{OH}}$ and $\nu_{3\text{OH}}$ stretching vibrations, both occur in
300 the 3600-2900 cm^{-1} region where as the bending mode $\nu_2 \text{ H}_2\text{O}$ ($\delta \text{ H}_2\text{O}$) appear in the

301 range 1700-1590 cm^{-1} [66]. A free tellurite ion, TeO_3^{2-} (C_{3v} symmetry) shows four
302 vibrational modes as ν_1 758 cm^{-1} , ν_2 364 cm^{-1} , ν_3 703 cm^{-1} and ν_4 326 cm^{-1} [67]. It
303 should be pointed out that there is little work has been done on tellurite minerals, in
304 particular, near-infrared spectroscopy.

305

306 *Hydroxyl stretching vibrations: 3800-2500 cm^{-1} spectral region*

307

308 Molecular water that is weakly hydrogen bonded absorbs in the range 3650-
309 3400 cm^{-1} . More strongly hydrogen bonded H_2O molecules are commonly
310 manifested as broad diffuse absorption bands below 3400 cm^{-1} [68]. Supplementary
311 information Figure 4a shows xocomecatlite OH stretching is strong in 3700-2800 cm^{-1}
312 region. Three prominent bands are observed at 3405, 3240 and 2920
313 cm^{-1} . Two lower intensity bands are observed at around 3100 cm^{-1} and are attributed
314 to hydrogen bonded water molecules. Tlapallite bands are shifted to longer
315 wavenumbers at 3640 and 2930 cm^{-1} . This shows molecular water is very weak in the
316 mineral tlapallite. Bands in the OH stretching region are not strong but the appearance
317 of sharp bands might be caused by many cations of Ca, Pb, Cu and Zn included in the
318 mineral structure. The IR bands of rodalquilarite (Supplementary information Figures
319 4c and 4d) are intense and appear to be shifted to low wavenumbers. This shift is
320 attributed to the presence of $(\text{H}_3\text{O})^+$ units in the structure. This results in stronger
321 hydrogen bonding and consequently bands are observed at lower wavenumbers. All
322 the three bands centred at 3380, 2755 and 2340 cm^{-1} exhibit many components. The
323 observation of H_2O stretching vibrations ν_{OH} shifted to low wavenumbers in
324 Xocomecatlite and rodalquilarite compared to tlapallite is the character of adsorbed
325 molecular water in the two tellurite minerals xocomecatlite and rodalquilarite. Raman
326 spectroscopy has been used to study the tellurite minerals teineite and graemite; both
327 contain water as an essential element of their stability [69]. For teineite prominent
328 Raman bands are observed at 3495, 3040, 2854 and 2286 cm^{-1} . In the Raman
329 spectrum of graemite, three Raman bands are reported at 3450, 3268 and 2937 cm^{-1} .
330 IR bands of OH stretching vibrations closely resemble with Raman data.

331

332 *H_2O bending vibrations ($\delta \text{H}_2\text{O}$): 1600-1300 cm^{-1} spectral region*

333 Bending vibrations δ H₂O observed in the spectra are depicted in
334 Supplementary information Figures 4b, 5a and 5b. A single band is centred at 1610
335 cm⁻¹ in tlallallite. For xocomecatlite
336 this band appears nearly at the same position 1630 cm⁻¹ but accompanied by three
337 more bands 1460, 1375 and 1330 cm⁻¹(Supplementary information Figure 5a). The δ
338 H₂O bending vibrations of rodalquilarite are well resolved at 1625, 1430 and 1390
339 with shoulder 1335cm⁻¹. The occurrence of more number of bands in the H₂O bending
340 vibrations region show non-equivalent types of molecular water in the minerals [68].

341

342 *Tellurite (TeO₃)²⁻ stretching vibrations: 1200-550 cm⁻¹ spectral region*

343 The IR bands of tellurite ion (TeO₃)²⁻ in the spectra of three tellurite minerals
344 are shown in Supplementary information Figures 6a to 6d. Xocomecatlite spectrum
345 shows main absorptions at 1070, 780 and 665 cm⁻¹. The most intense peak at 1070
346 cm⁻¹ with prominent components at 1135, 980 and 915 cm⁻¹ is identified as δ Te-OH
347 bending vibrations. Next to this feature, a pair of less intense bands at 780 and 755
348 cm⁻¹ are assigned to the ν_1 (TeO₃)²⁻ symmetric stretching mode. In low wavenumbers
349 one intermediate intensity band at 665 cm⁻¹ with splitting at 690 and 600 cm⁻¹ is
350 attributed to ν_3 (TeO₃)²⁻ antisymmetric stretching mode. The IR bands in tlallallite at
351 800 and 780 cm⁻¹ are attributed to the ν_1 (TeO₃)²⁻ symmetric stretching mode. A
352 group of three bands in the 700-600 cm⁻¹ region at 695, 675 and 590 cm⁻¹ are related
353 to the antisymmetric ν_3 modes of tellurite ion. The IR spectra of the two minerals
354 xocomecatlite and tlallallite are nearly identical. Rodalquilarite shows a complex
355 profile with overlapping of bands. The effect of iron is reflected in the spectrum by
356 appearing the vibrational modes of tellurite ion at different positions in rodalquilarite
357 H₃Fe₂(TeO₃)₄Cl. The bending vibrations of δ Te-OH display a small shift to high
358 wavenumbers whilst ν_1 and ν_3 modes of (TeO₃)²⁻ ion show splitting of components in
359 the wavenumbers at 840, 735, 675, 660, 625, 610, 600, 590 and 580 cm⁻¹. The report
360 on Raman spectroscopic study of tellurite minerals shows Raman bands for teineite at
361 739 and 778 cm⁻¹ and for graemite at 768 and 793 cm⁻¹ are assigned to the ν_1 (TeO₃)²⁻
362 symmetric stretching mode whilst bands at 667 and 701 cm⁻¹ for teineite and 676 and
363 708 cm⁻¹ for graemite are attributed to the ν_3 (TeO₃)²⁻ antisymmetric stretching mode.
364 Raman bands for teineite at 318 and 347 cm⁻¹ are assigned to the (TeO₃)²⁻ ν_2 (A₁)
365 bending mode and the two bands for teineite at 384 and 458 cm⁻¹ are assigned to the
366 (TeO₃)²⁻ ν_4 (E) bending mode. (TeO₃)²⁻ bending modes (ν_2 and ν_4) are not observed

367 here as they are below detectable limit of IR spectroscopy. Variable spectral
368 parameters of tellurites are used to identify three tellurite minerals investigated.

369

370 Conclusions

371

372 a) Two bands observed for Cu^{2+} ion in the near-infrared spectrum of xocomecatlite
373 at 1014 and 1109 nm (9855 and 9015 cm^{-1}) are assigned to ${}^2\text{B}_{1g} \rightarrow {}^2\text{B}_{2g}$ and ${}^2\text{B}_{1g}$
374 $\rightarrow {}^2\text{A}_{1g}$ transitions.

375

376 b) Cu^{2+} bands in tlalallite are distinctly appeared at 10690 cm^{-1} with two components
377 at 11490 and 9840 cm^{-1} and the second band shows shift to low wavenumbers at
378 7615 cm^{-1} .

379

380 c) Rodalquilarite is characterised by ferric ion absorption over the range 12300 - 8800
381 cm^{-1} . Both, tlalallite and rodalquilarite exhibit similar features in the range
382 8300 - 7400 cm^{-1} .

383

384 d) Three water vibrational overtones are observed in xocomecatlite at 7140 , 7075 and
385 6935 cm^{-1} where as in tlalallite bands are shifted to low wavenumbers at 7135 ,
386 7080 and 6830 cm^{-1} .

387

388 e) Bands in the 7240 - 6900 cm^{-1} region are attributed to the first overtones of ν_{OH}
389 vibrations of tellurites observed in the IR range 3650 - 2200 cm^{-1}

390

391 f) The appearance of the most intense peak near 5150 cm^{-1} with a pair of weak
392 shoulders at $\sim 5650\text{ cm}^{-1}$ a common feature in all the spectra, is related to the
393 combinations of OH vibrations of water molecules and bending vibrations.

394

395 g) The intensity of absorption feature with lowering of OH stretching band energies
396 confirms strong hydrogen bonding in xocomecatlite.

397

398 h) A number of overlapping bands are the combinational modes of $(\text{TeO}_3)^{2-}$ ion
399 observed in the low wavenumbers at 4800 - 4000 cm^{-1} . Distinct patterns

400 displayed by the minerals are utilised for rapid identification of the specific type
401 of tellurite mineral.

402

403 i) Bending vibrations δ H₂O observed at 1610 cm⁻¹ as a single peak in tlapallite split
404 into a number of components is the cause of non-equivalent types of molecular
405 water in xocomecatlite and rodalquilarite minerals.

406

407 j) The IR bands measured for the three tellurite minerals from three main absorptions
408 at 1080, 780 and 695 cm⁻¹ are attributed to the vibrational modes of (TeO₃)²⁻ ion
409 .The strongest peak centred at 1070 with prominent component bands at 1135,
410 980 and 915 cm⁻¹ is identified as δ Te-OH bending vibrations.

411

412

413 **Acknowledgements**

414

415 The financial and infra-structure support of the Queensland University of
416 Technology Inorganic Materials Research Program of the School of Physical and
417 Chemical Sciences is gratefully acknowledged. The Queensland University of
418 Technology is also acknowledged for the award of a Visiting Professorial Fellowship
419 to B. Jagannadha Reddy.

420

421

422

423

424

425

426 **References**

- 427 [1] J.D. Dana, Dana's Manual of Mineralogy, by W. E. Ford. 13th edition, Wiley,
428 London
- 429 [2] H. Effenberger, *Tschermaks Mineralogische und Petrographische*
430 *Mitteilungen* 24 (1977) 287-298.
- 431 [3] P. Du Ry, M. Fouassin, J. Jedwab, R. Van Tassel, *Annal.Soc. Geol. Belg.*
432 99 (1976) 47-60.
- 433 [4] A. Kato, K.-i. Sakurai, *Min. J.* 5 (1968) 285-290.
- 434 [5] A. Zemann, J. Zemann, *Acta Cryst.* 15 (1962) 698-702.
- 435 [6] A. Zemann, J. Zemann, *Beitr. Mineral. u. Petrog.* 7 (1960) 436-438.
- 436 [7] T. Yosimura, *J. Faculty Sci. Hokkaido Imp. Univ.* 4 (1939) 465-470.
- 437 [8] J. Moreau, *Bull. Soc. Franc.Min.Crist.* 98 (1975) 263-268.
- 438 [9] S.A. Williams, P. Matter, III, *Min. Rec.* 6 (1975) 32-34.
- 439 [10] J.W. Anthony, R.A. Bideaux, K.W. Bladh, M.C. Nichols, *Handbook of*
440 *Mineralogy, Volume V, Borates, Carbonates, Sulfates., Mineral Data*
441 *Publishing, Tuscon, Arizona, U. S. A., 2003.*
- 442 [11] R. Miletich, *Monat. Chem.* 126 (1995) 417-.
- 443 [12] M. Wildner, *Min. Petr.* 48 (1993) 215-225.
- 444 [13] N.S. Bhuvanesh, P.S. Halasyamani, *Inorg. Chem.* 40 (2001) 1404-1405.
- 445 [14] R. Miletich, *Euro. J.Min.* 7 (1995) 509-523.
- 446 [15] R.V. Gaines, *Univ. Nacl. Autonoma Mex., Inst. Geol. Bol.* 75 (1965) 1-15.
- 447 [16] R. Fischer, M. Schlatti, J. Zemann, *Anzeiger der Oesterreichischen Akademie*
448 *der Wissenschaften, Mathematisch-Naturwissenschaftliche Klasse* 5 (1969)
449 93-94.
- 450 [17] R.V. Gaines, *Am. Min.* 54 (1969) 697-701.
- 451 [18] A.C. Roberts, T.S. Ercit, A.J. Criddle, G.C. Jones, R.S. Williams, F.F.
452 *Cureton, II, M.C. Jensen, Min. Mag.* 58 (1994) 417-424.
- 453 [19] A.C. Roberts, M. Bonardi, J.D. Grice, T.S. Ercit, W.W. Pinch, *Can. Min.* 27
454 (1989) 129-131.
- 455 [20] O. Lindqvist, *Acta Chem. Scand.* 22 (1968) 977.
- 456 [21] K. Hanke, *Naturwissenschaften* 53 (1966) 273.
- 457 [22] K.K. Hanke, V.; Lindqvist, O.;, *Acta Crystallogr.* B29 (1973) 963.
- 458 [23] J.W.K. Christopher R. Ferger, *Inorg. Chem.* 37 (1998) 4046-4051.
- 459 [24] S.A.M.D. Williams, *Min. Mag.* 42 (1978) 183-186.
- 460 [25] S.A. Williams, *Min. Mag.* 40 (1975) 221-226.
- 461 [26] R.L. Frost, M.J. Dickfos, *J. Raman Spec.* 38 (2007) 1516-1522.
- 462 [27] R.L. Frost, J. Cejka, *J. Raman Spec.* 38 (2007) 1488-1493.
- 463 [28] A.J. Locke, W.N. Martens, R.L. Frost, *J. Raman Spec.* 38 (2007) 1429-1435.
- 464 [29] R.L. Frost, J. Cejka, G.A. Ayoko, M.L. Weier, *J. Raman Spec.* 38 (2007)
465 1311-1319.
- 466 [30] R.L. Frost, J.M. Bouzaid, *J. Raman Spec.* 38 (2007) 873-879.
- 467 [31] R.L. Frost, C. Pinto, *J. Raman Spec.* 38 (2007) 841-845.
- 468 [32] R.L. Frost, M.L. Weier, P.A. Williams, P. Leverett, J.T. Kloprogge, *J. Raman*
469 *Spec.* 38 (2007) 574-583.
- 470 [33] R.L. Frost, J. Cejka, M.L. Weier, *J. Raman Spec.* 38 (2007) 460-466.
- 471 [34] R.L. Frost, J. Cejka, M.L. Weier, W.N. Martens, G.A. Ayoko, *J. Raman Spec.*
472 38 (2007) 398-409.
- 473 [35] R.L. Frost, J.M. Bouzaid, W.N. Martens, B.J. Reddy, *J. Raman Spec.* 38
474 (2007) 135-141.

- 475 [36] R.L. Frost, S.J. Palmer, J.M. Bouzaid, B.J. Reddy, *J. Raman Spec.* 38 (2007)
476 68-77.
- 477 [37] B.J. Reddy, R.L. Frost, *Neues Jahrb. Mineral., Monatsh.* (2004) 525-536.
- 478 [38] B.J. Reddy, F. Nieto, A.S. Navas, *Neues Jahrb. Mineral.*, (2004) 302-316.
- 479 [39] R.L. Frost, R.-A. Wills, W. Martens, M. Weier, B.J. Reddy, *Spectrochim.*
480 *Acta*, 62A (2005) 42-50.
- 481 [40] B.J. Reddy, L. Frost Ray, *Spectrochim Acta* 61 (2005) 1721-1728.
- 482 [41] B.J. Reddy, R.L. Frost, W.N. Martens, *Mineral. Mag.* 69 (2005) 155-167.
- 483 [42] M.L. Weier, R.L. Frost, B.J. Reddy, *J. Near Infrared Spectrosc.* 13 (2005) 359-
484 369.
- 485 [43] R.L. Frost, B.J. Reddy, W.N. Martens, M. Weier, *J. Mol. Struct.* 788 (2006)
486 224-231.
- 487 [44] B.J.R. R.L. Frost, D.L. Wain and M.C. Hales, *J. Near infrared Spectrosc.* 14
488 (2006) 317-324.
- 489 [45] L.M. Daniel, R.L. Frost, H.Y. Zhu, *J. Coll.Inter. Sc.* 316 (2007) 72-79.
- 490 [46] B.J. Reddy, R.L. Frost, *J. Near Infrared Spectrosc.* 15 (2007) 115-121.
- 491 [47] B.J. Reddy, R.L. Frost, *Spectrochim. Acta*, 66A (2007) 312-317.
- 492 [48] B.J. Reddy, R.L. Frost, W.N. Martens, D.L. Wain, J.T. Klopogge, *Vib.*
493 *Spectrosc.* 44 (2007) 42-49.
- 494 [49] V. Vagvoelgyi, S.J. Palmer, J. Kristof, R.L. Frost, E. Horvath, *J. Coll.Inter. Sc.*
495 318 (2008) 302-308.
- 496 [50] B.J.R. Ray L Frost, Eloise C. Keeffe, , *J. Near Infrared Spectrosc.* 2008, xxx.
- 497 [51] G.R. Hunt, J.W. Salisbury, *Mod. Geol.* 2 (1971) 23-30.
- 498 [52] D.E. Billing and B.J. Hathaway, *J. Chem. Soc. (A)* (1968) 1516-1519.
- 499 [53] C.J. Ballhausen, McGraw-Hill Book Co., Inc., New York (1962).
- 500 [54] A.B.P. Lever, *Studies in Physical and Theoretical Chemistry, Vol. 33:*
501 *Inorganic Electronic Spectroscopy.* 2nd Ed, 1984.
- 502 [55] B.J. Hathaway, D.E. Billing, *Coord. Chem. Rev.* 5 (1970) 143-207.
- 503 [56] P. Sreeramulu, K.M. Reddy, A.S. Jacob, B.J. Reddy, *J. Crystallogr. Spectrosc.*
504 *Res.* 20 (1990) 93-96.
- 505 [57] K.B.N. Sarma, B.J. Reddy, S.V.J. Lakshman, *Phys. Lett.* 92A (1982) 305-308.
- 506 [58] R. L. Frost, Jagannadha Reddy, B., Wain, D.L., 16 (2008) 75-82.
- 507 [59] G.R. Rossman, *Min. Spectrosc.* 5 (1996) 23-27.
- 508 [60] G.R.S. Hunt, J.W.; Lenhoff, C.J., *Mod. Geol.* 2 (1971) 195-205.
- 509 [61] R.N. Clark, King, T.V.V., Klejwa, M., Swayze, Vergo, N., *J. Geophys. Res.*
510 95 (1990) 12653-12680.
- 511 [62] R.L. Frost, B. J.;Reddy, E.C. Keeffe, *Journal of Near Infrared Spectroscopy*
512 (2008 (communicated)).
- 513 [63] M.L. Welch, G., *Am. Min.* 88 (2003) 1401.
- 514 [64] R.E.M. Milliken, J.F., *Icarus* 189 (2007) 574-588.
- 515 [65] E.R. Libowitzky, G.R., *Am. Min.* 82 (1997) 1111-1115.
- 516 [66] K. Nakamoto, (1986).
- 517 [67] V.C. Farmer, *Mineralogical Society Monograph 4: The Infrared Spectra of*
518 *Minerals*, 1974.
- 519 [68] P.C. Burns, Finch, R., 38 (1999) 499-577.
- 520 [69] S.L. Reddy, M. Fayazuddin, N.C.G. Reddy, T. Endo, R.L. Frost, *Radiation*
521 *Effects and Defects in Solids* 163 (2008) 19-27.
522
523

524
525

S. No.	Name	Formula	Structure	Origin
1	Xocomecatlite	$\text{Cu}_3[(\text{OH})_4\text{TeO}_4]$	Orthorhombic	Bambollita Mine, Moctezuma District, Sonora, Mexico
2	Tlapallite	$\text{H}_6(\text{Ca,Pb})_2(\text{Cu,Zn})_3\text{SO}_4(\text{TeO}_3)_4\text{TeO}_6$	Monoclinic	Bambollita Mine, Moctezuma District, Sonora, Mexico
3	Rodalquilarite	$\text{H}_3\text{Fe}_2(\text{TeO}_3)_4\text{Cl}$	Triclinic	Wendy Pit, El Indio Gold Mine, Coquimbo, Chile

526
527
528
529
530
531
532

Table 1 Table of the tellurite minerals, their chemical formula and origin, used in this study

Xocomecatlite Cu ₃ [(OH) ₄ TeO ₄] (Mexico) v (cm ⁻¹) [Present study]	Tlapallite H ₆ (Ca,Pb) ₂ (Cu,Zn) ₃ SO ₄ (TeO ₃) ₄ TeO ₆ (Mexico) v (cm ⁻¹) [Present study]	Rodalquilarite H ₃ Fe ₂ (TeO ₃) ₄ Cl (Chile) v (cm ⁻¹) [Present study]	Chalcomenite Cu[SeO ₃] ₂ ·2H ₂ O (Bolivia) v (cm ⁻¹) [Reported [59]]	Chalcomenite Cu[SeO ₃] ₂ ·2H ₂ O (Canada) v (cm ⁻¹) [Reported [59]]	Clinochalcomenite Cu[SeO ₃] ₂ ·2H ₂ O (Bolivia) v (cm ⁻¹) [Reported [59]]	Suggested assignment
11560c 10835c 9855	11490c 10690 9840c	- - -	11300c 9935 9065c	11830c 11245 9980c	11225c 10380 9050c	² B _{1g} → ² A _{1g} ^{t1}
-	-	11230c 10460	-	-	-	⁶ A _{1g} → ⁴ T _{1g} ^{t2}
9015	7990c 7615	7910 7585c 7405w	8585	8675	8560	² B _{1g} → ² B _{2g} ^{t1}
7240sh 7140c 7075 6935sh	7135 7080	7185c 7010	6950sh	~6900sh	7040sh	2v ₃ ^a
6825c	6830	6855sh	6810	~6800	6810	2v ₁ ^a

6755w 6685	6640	6765 6660sh 6545c				
-	-	-	6700	~6700 6210c 6090w	6695	$(\text{SeO}_3)^{2-} \cdot \text{H}_2\text{O}$
6375w 6060	6130	6325 6100	-	-	-	$(\text{TeO}_3)^{2-} \cdot \text{H}_2\text{O}$
5635	5630	5650 5470sh 5375c	5900sh 5640 5480c	5740sh 5595	5725sh 5630 5540c	$(\nu_3 + \nu_1)^a$
5240c 5150 5070c	5240c 5165 5060	5120c 4980sh	5170 5070sh	5170 5090sh	5170 5020sh	$(\nu_3 + \nu_2)^a$
4935sh	4920sh	-	4835	4840	4740	$(4\nu_1 + 3\nu_2)^b$
4755	4765	4820	-	-	-	$(5\nu_1 + 3\nu_2)^c$
4555	4550 4470	4610 4600	-	-	-	$(5\nu_1 + 2\nu_2)^c$

-	-	4520c	4470	4505sh 4420	4545	$4\nu_1+2\nu_2$ ^b
4270sh 4115	4270 4025	4305 4170sh 4110 4050c	-	-	-	$(4\nu_1 + 3\nu_2)$ ^c
-	-	-	4100c 4075	4240c 4085	4110sh 4075 4020	$(3\nu_1 + 2\nu_3)$ ^b

^{t1} Electronic transition of Cu²⁺

^{t2} Electronic transition of Fe³⁺

^a Overtones and combination modes of water stretching vibrations: $\nu_3 = 3650-3200$, $\nu_2 = 1610-1335$ and $\nu_1 = 3200-2200 \text{ cm}^{-1}$

^b Overtones and combination modes of (SeO₃)²⁻ fundamentals: $\nu_1 = 820-770$, $\nu_2 = 580-470$, $\nu_3 = 800-665$ and $\nu_4 = 400-360 \text{ cm}^{-1}$

^c Overtones and combination modes of (TeO₃)²⁻ fundamentals: $\nu_1 = 840-735$, $\nu_2 = 350-320$, $\nu_3 = 695-580$ and $\nu_4 = 460-380 \text{ cm}^{-1}$
Abbreviations: c-component; sh-shoulder; w-weak

Table 2 Assignments of the observed bands (cm⁻¹) in the near-infrared spectra of tellurite minerals: xocomecatlite, tlalallite and rodalquilarite and in comparison with selenite minerals of chalcogenites

List of Tables

Table 1 Table of the tellurite minerals, their chemical formula and origin, used in this study

Table 2 Assignments of the observed bands (cm^{-1}) in the near-infrared spectra of tellurite minerals: xocomecatlite, tlapallite and rodalquilarite and in comparison with selenite minerals of chalcomenites

List of Figures

Figure 1 NIR spectrum of xocomecatlite, tlapallite and rodalquilarite in the NIR high wavenumber region.

Figure 2 NIR spectrum of xocomecatlite, tlapallite and rodalquilarite in the NIR 8200-6400 cm^{-1} region.

Figure 3 NIR spectrum of xocomecatlite, tlapallite and rodalquilarite in the NIR 6500-4000 cm^{-1} region.

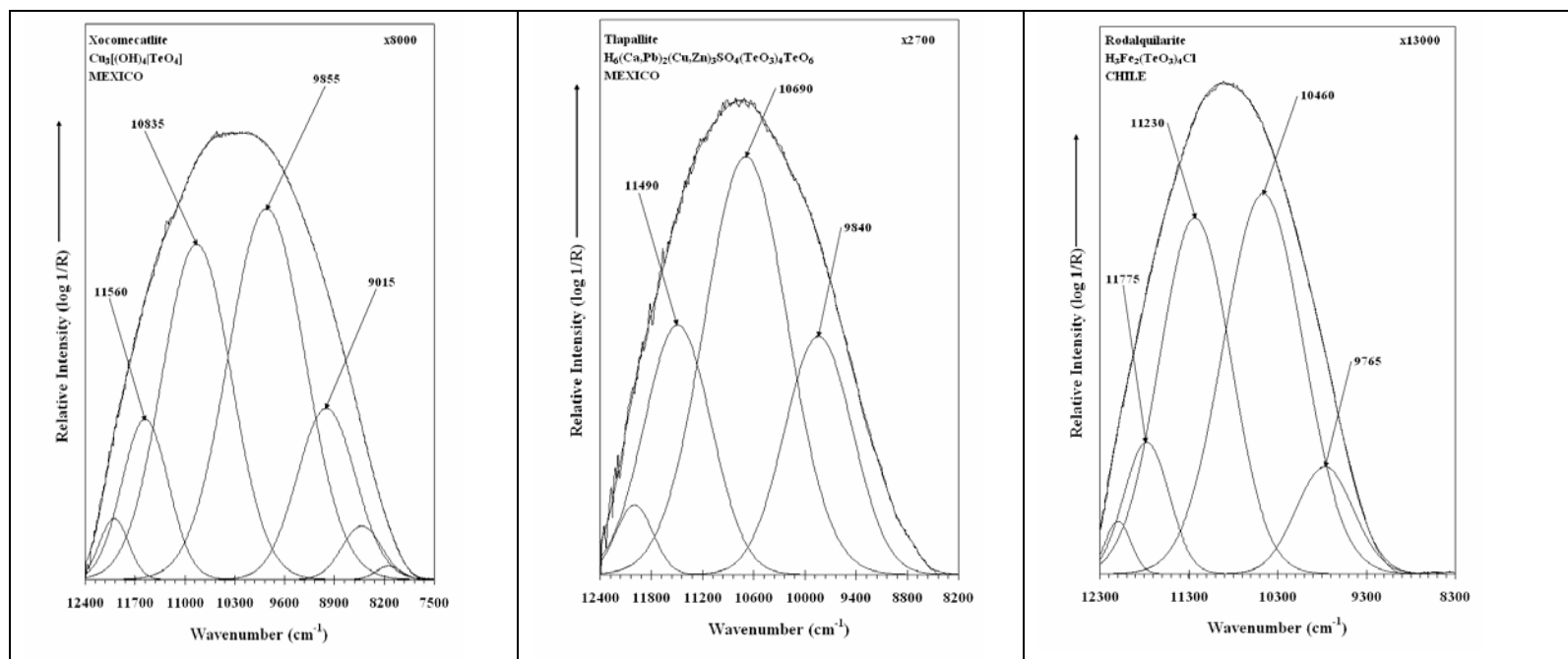


Figure 1 NIR spectrum of xocomecatelite, tlapallite and rodalquilarite in the high NIR wavenumber region.

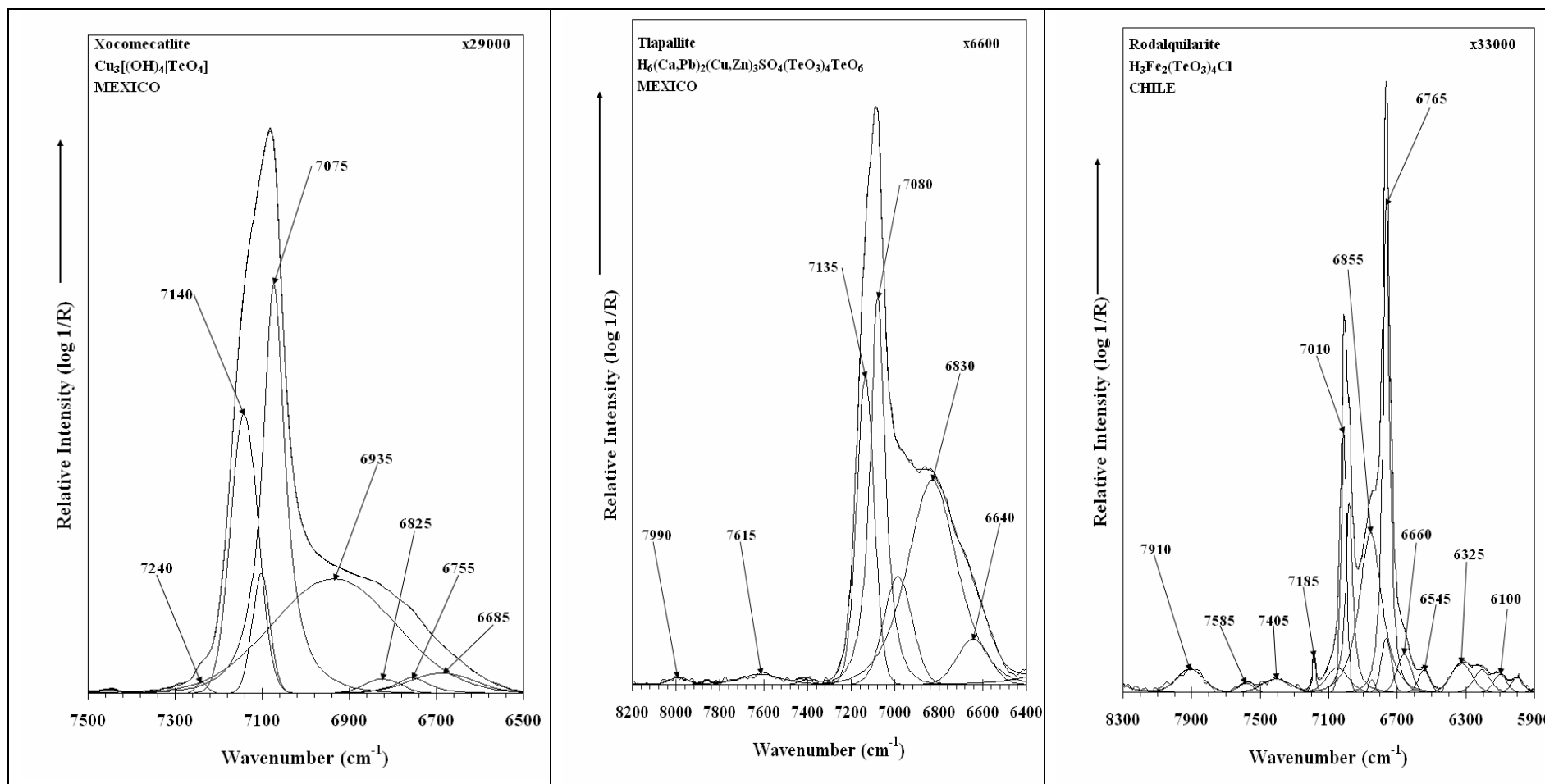


Figure 2 NIR spectrum of xocomecatlite, tlapallite and rodalquilarite in the 8200-6400 cm^{-1} region.

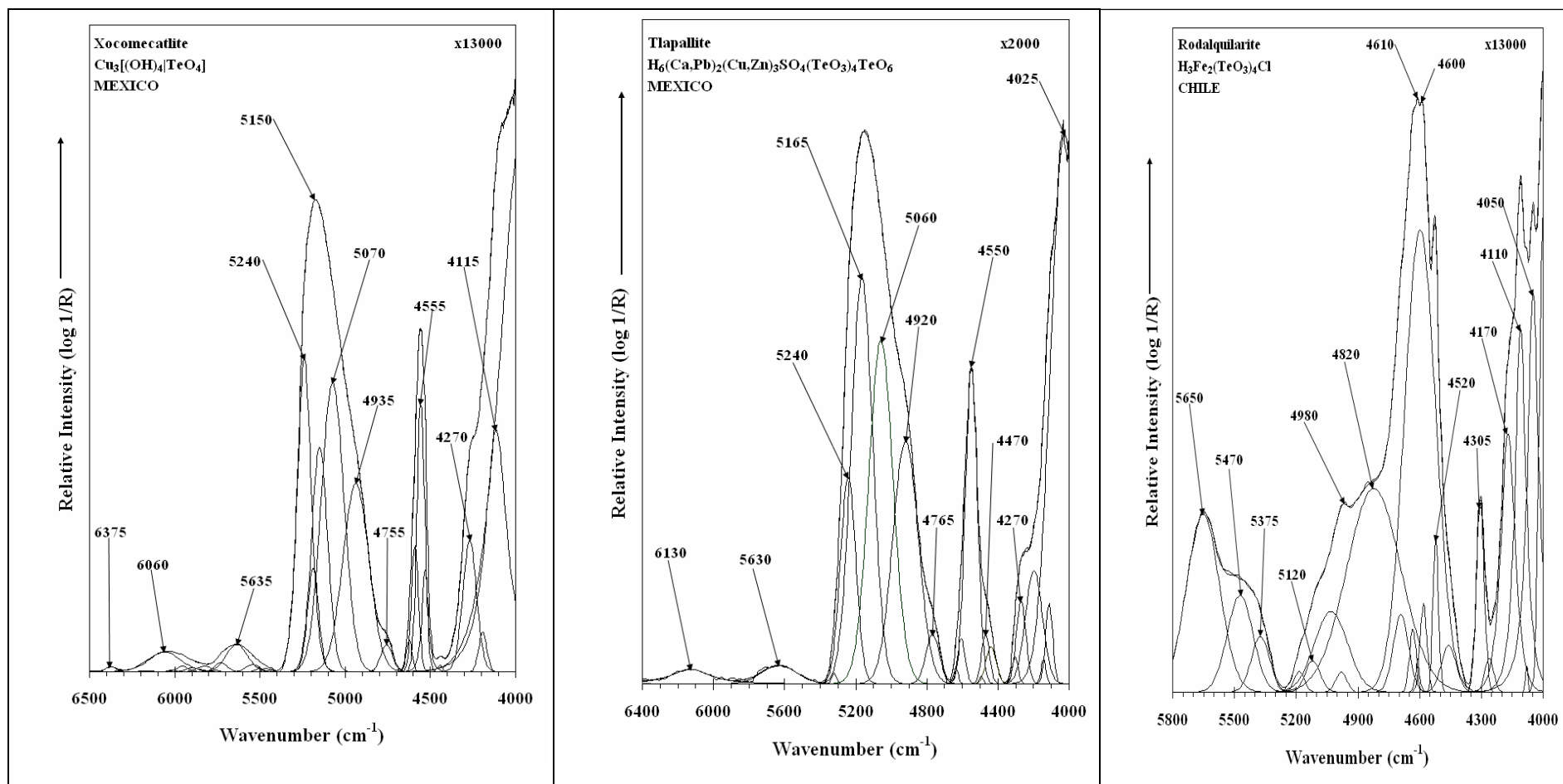


Figure 3 NIR spectrum of xocomecatlite, tlapallite and rodalquilarite in the NIR 6500-4000 cm^{-1} region.

